Electrical Power and Energy Systems 97 (2018) 138–145

Contents lists available at ScienceDirect

Electrical Power and Energy Systems

journal homepage: www.elsevier.com/locate/ijepes

Electrical operation behavior and energy efficiency of battery systems in a virtual storage power plant for primary control reserve

Christopher Betzin[a,b,*], Holger Wolfschmidt[a], Matthias Luther[b]

[a] Siemens AG, 91058 Erlangen, Germany
[b] University of Erlangen-Nuremberg, 91058 Erlangen, Germany

ARTICLE INFO

Keywords:
Lithium-ion batteries
Battery storage system efficiency
Primary control reserve
Battery system modeling

ABSTRACT

A rising interest in battery systems for various applications needs a deep understanding of the system performance for technical and economical optimization. The electrical system behavior and the energy efficiency of two different Li-ion battery systems are presented in this paper. Both systems are designed for operation in a virtual storage plant with respect to the primary control reserve. The efficiency of both systems is analyzed including the battery, the power electronics and auxiliary units. Based on the overall energy efficiency of the electrical storage systems, a model is developed to show the impact on the operation and standby behavior. This model is transferred in a simulation framework investigating the application of battery systems towards primary control reserve. Real frequency data of continental European transmission system are used to simulate the behavior of the two systems in order to determine energy losses during operation. Primary control reserve is one possible application as grid support service for battery systems and is under current discussion. In this new field of battery application energy losses are a limiting factor for economic and technical qualification. The simulation identifies strengths and weaknesses of the investigated systems based on the determined efficiencies, and the results support an optimized operation strategy.

1. Introduction

In a progressive developing society with increasing energy consumption, a need of flexibility and also with respect to ecologic values a global change of energy supply is required. A significant increase of the share of renewable energy in the coming years is expected [1]. Renewable energy supply and energy demand do not correlate inevitably. One way to solve this non-congruence is to store the energy. Therefore different storage technologies exist, e.g. battery storage systems with lithium ion battery cells.

Assuming a decrease of the number of central power plants for base load supply decentralized electrical power supply systems may play a dominant role in the future [2]. In order to manage these changes, storage solutions may contribute to support the necessary grid services which were previously provided by conventional power plants. For dispersed generation a larger number of small units will come into focus with new capabilities and uncertainties in operation. In any event the electrical grid has to be stabilized in short- and long-term time frames. For the short term application the primary control reserve is the symmetric control strategy to stabilize the grid to 50 Hz.

In order to stabilize electrical grids via primary control reserve lithium ion battery storage systems [3,4] can be used. The lithium ion technology is a promising storage technology due to high charge and discharge capabilities, high energy density and low self discharge. It is important to reach the highest possible efficiency in order to avoid the loss of energy, independent of the storage technology. Battery systems for primary control reserve are complex compared to standard stationary battery system for low power applications. Additional protection and controller units are necessary. However, additional devices consume additional energy and thus reduce the system efficiency. Therefore an economic successful operation of battery systems necessitates a detailed investigation of the efficiency behavior.

Primary control reserve cannot be provided by each system available on the market. The threshold performance for primary control reserve power is 1 MW. Thus, small systems such as in residential applications could only participate in the primary control reserve market as a pool of small systems called virtual power storage plant. In this case new possibilities arise. If different kinds of energy storage systems are integrated in this virtual storage plant, an optimization could be done with respect to advanced operation strategies. In this case it is also necessary to determine the efficiency depending on the power of each system. Auxiliary and standby losses are included in the efficiency in

* Corresponding author at: Siemens AG, 91058 Erlangen, Germany.
E-mail address: c.betzin@gmx.de (C. Betzin).

https://doi.org/10.1016/j.ijepes.2017.10.038
Received 15 February 2017; Received in revised form 29 September 2017; Accepted 30 October 2017
Available online 08 November 2017
0142-0615/

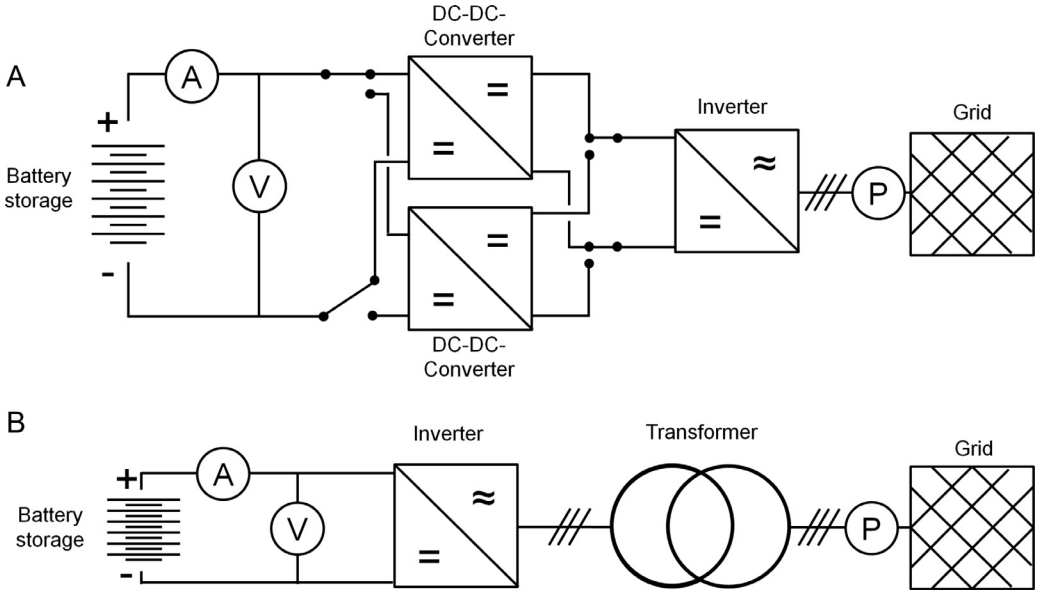

Fig. 1. Circuit diagrams of two different topologies of Battery-storage systems for primary control reserve including voltage, current and power measurements. (a) Battery-storage system with two DC-to-DC-converters with different maximum power and one DC to AC inverter and (b) battery-storage system with one DC to AC inverter and one transformer.

order to optimize each system within the power plant and to reduce energy consumption by supporting the grid.

In this paper two storage systems based on lithium ion technology are investigated relating to their application in the primary control reserve power market. The energy efficiency behavior and the energy losses are investigated and mathematical correlations are derived which were used to model both systems. The energy losses were determined under operation with respect to the primary control reserve.

2. Theory & experimental setup

Two different battery storage systems based on lithium ion technology for grid primary control reserve were investigated. Both systems have a maximum power of 20 kW, but consist of different system topologies. The equivalent circuit diagrams of both systems are shown in Fig. 1. System A had a direct current (DC) voltage level between 150 and 180 V with lithium ion cells, 25 A h each. The cells were graphite based on the anode side and NMC-oxide (lithium nickel manganese cobalt oxide) based on the cathode side. Three battery modules were installed in series whereby each module consisted of 15 cells in series connection and three in parallel (15s3p) with an energy content of 12 kWh. Two DC-to-DC converters for different power ranges were installed to set the DC link voltage to a higher level for the inverter to convert DC to a three-phase alternating current (AC) with a phase to phase voltage of 400 V. System B had a DC voltage level between 420 V and 560 V. Lithium ion cells with a graphite based anode and a NCA-oxide (lithium nickel cobalt aluminum oxide) based cathode were used, each cell having a capacity of 45 A h. The battery system consisted of 10 modules in series connection, where each module includes 14 cells in series. The energy content of the system was 20 kWh. One inverter was installed to convert DC link voltage to three phase AC voltage. Due to the level of the DC intermediate circuit voltage being too low to reach the phase to phase AC grid voltage of 400 V, a wye connected transformer was installed for direct grid connection. An overview of system A and system B is provided in Table 1.

Table 1
Rated power and energy of system A and B.

	System A	System B
Rated power/kW	20	20
Rated energy/kWh	12	20

The measurement points for voltage (V), current (A), and active power (P) are indicated. Both systems were investigated on the DC side via current sensors and voltage measurement and on the AC side via a 3 phase power measurement device (ECS-PM3-80) to determine the system parameters for characterization such as efficiency, auxiliary losses, standby losses and grid power. The DC voltage on both systems was measured with a LEM current transducer HTR 100-SB connected to a Keithley 2010 multimeter. The DC voltage was measured by the internal battery management system.

One of the key performance indicators of a storage system is the energy efficiency. Losses occur in the inverter, the battery, the transformer and in the auxiliary units.

$$\eta_t(P,\mathrm{SOC}) = \eta_b \eta_{el} \tag{1}$$

According to Eq. (1) system efficiency is divided into battery efficiency and electrical efficiency including everything other than the battery.

Essentially, the definition of efficiency of the total system η_t is the relationship between the energy supplied and the energy needed from the grid to re-establish the same state of charge (SOC) prior to the discharge (Eq. (2)).

$$\eta_t(P,\mathrm{SOC}) = \frac{\int_{SOC2}^{SOC1} |P_{g,d}|\,dt_d}{\int_{SOC1}^{SOC2} |P_{g,c}|\,dt_c} \tag{2}$$

In this equation $P_{g,d}$ is the power at the grid access point during the discharging and $P_{g,c}$ is the power at the grid access point during the charging process. For the time t the same indices are used. The limits of integration SOC1 and SOC2 describe the states of charge between which the measurements were carried out in order to determine the efficiency. The starting SOC was also the SOC at the end of the measurements in order to fulfill the definition.

For the determination of the energy storage efficiency it was also necessary to determine the auxiliary and standby losses, because these effects reduced the stored energy depending on storage time. These losses were included in η_{el} during operation and separately considered during the standby or 'Off' mode and they are listed in Section 3 in an overview.

2.1. Determination of system efficiency at a fixed SOC

In order to reduce the efforts to determine the system efficiency according to Eq. (2) an alternative approach to full charge/discharge cycles is proposed. For primary control as grid support service

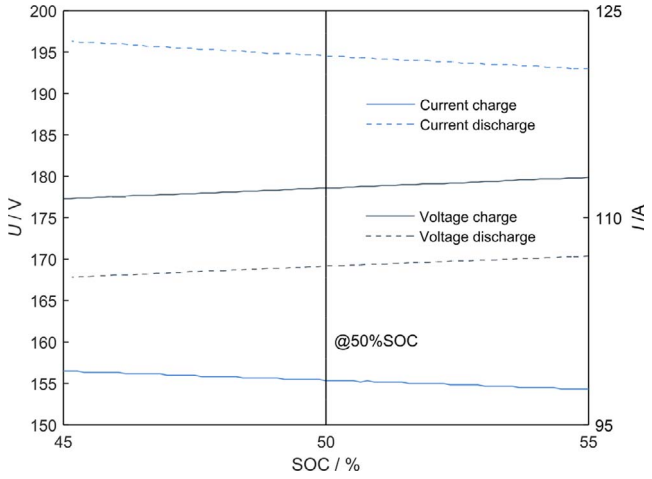

Fig. 2. Efficiency measurement with constant charge und discharge power of 19 kW at 50% SOC. Blue lines show current behavior grey lines show voltage behavior, while solid lines represent the charge mode and dashed lines the discharge mode. (For interpretation of the references to colour in this figure legend, the reader is referred to the web version of this article.)

symmetrically power provision has to be ensured. Thus, the battery state of charge (SOC) has to be around 50% SOC. Therefore, in this study 50% SOC was used as subject of investigation as shown in Fig. 2 with voltage and current behavior for constant charge and discharge power at the grid access point. It is important to remark, that this approach is not limited to this SOC. Although differences in internal resistances, especially at low and high SOC [5,6] are known, 50% SOC is representative for system description. The following considerations theoretically confirm that this assumption is more than reasonable. These relationships could also be used to determine the efficiency during operation particularly with respect to the lifetime of the system, to determine indirect aging effects, which occur in lithium-ion batteries [7–25]. Eq. (2) is used for the power depending overall efficiency. The power from and to the grid was constant for each measurement: $P_{g,d} = P_{g,c}$. One further definition is that the capacity of battery system is equal for charging and discharging in a specific state of charge range: $|I_{b,d}\,t_{b,d}| = |I_{b,c}\,t_{b,c}|$. Substitution of this definition into Eq. (2) results in the following equation:

$$\eta_t(P,\mathrm{SOC}) = \frac{|I_c|}{|I_d|} \tag{3}$$

The overall efficiency at a specific state of charge with constant power on the grid could be determined with this equation by the ratio of the current in the battery during charging and discharging.

The efficiency of the battery system is not only the cell efficiency, but also cell connection, BMS electronics and energy supply need to be factored in. In order to determine the battery system efficiency the following equation based on the consideration, that the energy from the battery divided by energy into the battery is the efficiency of the battery system with constant power on grid, is formulated:

$$\eta_b(P,\mathrm{SOC}) = \frac{\int_{SOC2}^{SOC1} P_{b,d}\,t_{b,d}}{\int_{SOC1}^{SOC2} P_{b,c}\,t_{b,c}} = \frac{U_{b,d}\,I_{b,d}\,t_{b,d}}{U_{b,c}\,I_{b,c}\,t_{b,c}} \tag{4}$$

If the diffusion processes are in equilibrium without a diffusion gradient, and thus in first order stationary, the equation could be reduced by the assumption of $|I_{b,d}\,t_{b,d}| = |I_{b,c}\,t_{b,c}|$ to the following equation at specific SOC and P:

$$\eta_b(P,\mathrm{SOC}) = \frac{U_{b,d}(\mathrm{SOC})}{U_{b,c}(\mathrm{SOC})} \tag{5}$$

In this case the round trip efficiency can be estimated from the ratio of battery voltages although no complete charge and discharge cycle were performed. In order to determine electrical losses for systems such as power electronics and control units with energy supply during operation Eq. (1) is used.

$$\eta_{el}(P,\mathrm{SOC}) = \frac{\eta_t}{\eta_b} \tag{6}$$

Eq. (6) is substituted by Eqs. (3) and (5), and following equation is obtained under the condition that $P_{g,c} = P_{g,d}$:

$$\eta_{el}(P,\mathrm{SOC}) = \frac{\eta_t}{\eta_b} = \frac{I_c\,U_{b,c}}{I_d\,U_{b,d}} = \frac{|P_{b,c}|}{|P_{b,d}|} \tag{7}$$

The efficiency of the electronics can be determined by measuring the power during charging and discharging at the battery if the power at the grid access point is the same for charge and discharge.

Based on the previous conclusions the measurements for the energy efficiency determination were performed by voltage, current and power analysis, shown in Fig. 2. The graph shows the voltage and the current of system A with constant charge und discharge power of 19 kW at 50% SOC. The solid lines show the results while charging and the dashed lines while discharging. The blue lines are the current measurement with decreasing current with increasing state of charge level, and the grey lines show the voltage measurement with increasing voltage at increasing SOC. In addition, the three phase AC power measurements between the grid and battery energy storage system were carried out to review the measurements.

The supply of primary control reserve depends on the grid frequency and can be provided positively or negatively. In order to provide the required minimum of 1 MW reserve power [26] with small decentralized battery storages such as the two investigated systems, a virtual storage plant has to be set up. Each system which participates at the primary control reserve market has to react between 49.8 and 50.2 Hz and should able to supply positive as well as negative full load within 30 s and support the grid for a maximum of 15 min with constant power. In Fig. 3 the deadband of ± 10 mHz around 50 Hz is shown, and a maximum power of 20 kW for negative and positive response for the particular frequency is shown which represents the maximum power of the investigated systems. A linear relationship between the frequency and the active power is assumed.

3. Experimental results

The experimental section is divided into three parts. In the first part the results on energy efficiency of both systems are presented, separated in total, battery and electrical system efficiency. The second part discusses the influence of the state of charge dependency of the total energy efficiency according to constant power mode. The third part

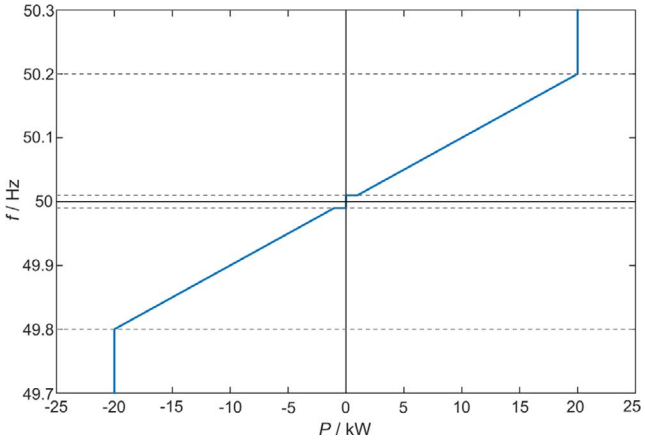

Fig. 3. Frequency power function for primary control reserve provided by a 20 kW battery system according to the German Transmission code [26] including a deadband of ± 10 mHz.

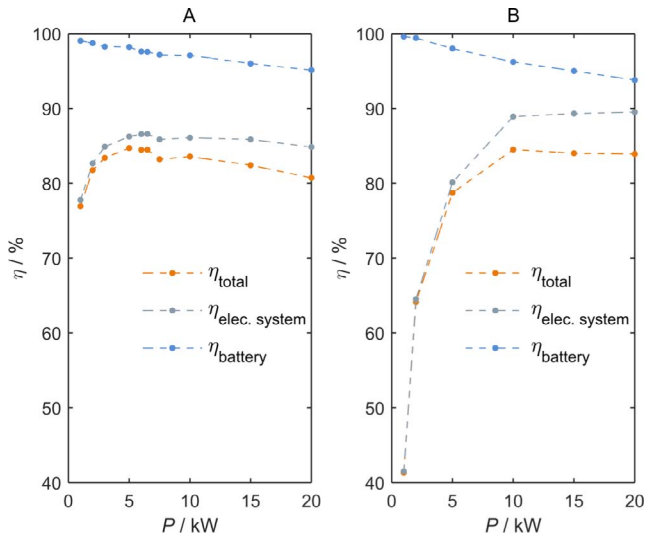

Fig. 4. Power dependent round-trip efficiencies of two different Li-Ion battery-storage systems for system A and system B. The orange lines show the overall or total efficiency, the blue lines battery efficiency and the grey lines the efficiency of power electronics including energy supply and auxiliary losses. (For interpretation of the references to colour in this figure legend, the reader is referred to the web version of this article.)

describes the investigation of system operating conditions.

In Fig. 4 the results of the round trip efficiency versus power for system A and B are shown. On the left hand side the results of system A and on the right hand side the results of system B are presented. The blue lines represent the results of the battery system efficiency. The efficiency includes the cell efficiency and losses which occurred in the battery modules up to the DC intermediate circuit at the inverter. The grey lines represent the system losses, which included the power electronics, control devices and the auxiliary power supply. The orange lines show the total system efficiency including all above mentioned losses.

The results shown in Fig. 4 exhibit a decisive difference in system behavior depending on the power range. The important key figure is the total efficiency. System A showed a higher efficiency in the lower power range up to 7 kW compared to system B. System B had a higher efficiency beyond a power range of 7 kW. The graph of battery system efficiency could be described as a linear function with a different slope for each system, due to different battery system topology, energy content and cell specification.

The battery system behavior was described by three major aspects: cell chemistry, internal cell setup and system configuration. System A had a NMC-based cathode cell, which has a high rate performance [27] which is advantageous for high power demand compared to system B with a NCA based cathode. NCA has a higher resistance with cycling and a poor behavior at high C-rates [28] compared to NMC-based cells. Both systems contained cells which are energy optimized but the two cell types differed by capacity and probably by active material constitution, such as thickness, which influences the internal resistance [29,30]. Cells in system A had a capacity of 25 A h and in system B of 45 A h. Nevertheless system B consisted of 140 cells in a 10 module 14 s design whereas system A contains of 135 cells with a 3 module 15s3p design. At lower power range system B had a similar efficiency at battery system level compared to system A (see Fig. 4). At higher power system B showed a lower efficiency which was caused by higher resistance effects. The linear efficiency versus power behavior of both systems was almost only influenced by ohmic effects, which are linearly dependent on current [31].

The system efficiency strictly depends on the electrical configuration. System A had two bidirectional DC-DC-converter for different power ranges (see Fig. 1). The bigger the difference of the voltage ratio is the larger the efficiency drop is [32]. Switching losses and conductor losses occur at higher frequency levels and high currents [33]. Therefore efficiency decrease occurs at higher power level [34], which is also seen in Fig. 4. In this case the system efficiency of System A was dominated by the behavior of the DC-DC-converter. The switching between the two DC-to-DC converters was around 7 kW (see Fig. 4). Due to the constant voltage output of the DC/DC converter to the AC/DC converter, the voltage dependency of the efficiency is not given. Only the power range had an impact on the AC/DC converter efficiency. Unsymmetrical efficiency behavior caused by bidirectional switching [35] was not considered in this study.

System B showed a completely different system efficiency behavior with respect to the power level. For this concept typical high frequency inverter efficiency was observed. The point of peak efficiency was in the higher power range beyond 10 kW. The system efficiency curve was dominated by the inverter efficiency. At higher power and thus higher currents conductor losses increased and the efficiency decreased. At lower power range lower conversion efficiency of system efficiency was obtained, caused by standby and auxiliary losses of the inverter [36], which is also valid for system A.

System B had a wye-connected 1/1.45 transformer to directly connect the battery storage system to the grid. The frequency range of the transformer was in a known bandwidth, for primary control reserve between 49.8 and 50.2 Hz. Hysteresis losses and eddy current, which are typical losses were proportional to the frequency or its square. These losses were almost power independent and thus did not have a strong impact on the system efficiency. In general, also losses based on magnetic flux and copper losses are depended on current and power [37]. On the basis of a small transformer winding ratio and therefore a small current ratio, the power dependency could be neglected.

The total system efficiency of both systems was a function of battery losses and system losses caused energy supply and power electronics with control units. The dominant parts of losses depending on the power range were power electronic losses depending on each system topology. The battery losses were relative small compared to the power electronic losses.

As mentioned before, lithium ion batteries have an internal resistance, which depends on the state of charge [38,39] and show an increased internal resistance at low and high SOCs. Therefore the influence of the state of charge dependency on the overall system efficiency is discussed in order to describe the cell effects on system level and to be sure that the cells are not operated at their SOC limits. Due to different currents at constant power mode, the DC parts could also be influenced. Thus, the overall battery storage efficiency could be affected. The different currents versus SOC are shown in Fig. 2 for the range of SOC around 50%.

In Fig. 5 the results of the state of charge dependency of the battery storage system are shown for system A at constant power mode of 15 kW. The charge process at constant power level of 15 kW on grid is pictured with solid lines, the discharge process with dashed lines. The state of charge between 0% and 100% was the usable SOC provided by system A. This SOC was not determined at the battery cell level, a recalculation to the battery SOC lead to values between 6% and 87%. The grey lines illustrate the power on grid; blue lines are the battery power depending on the state of charge. The orange lines are the difference between the power on the grid and the power on the battery, which represents the losses, occurring due to the power electronics and the additional energy supply of the overall system. During discharge a higher power level of the battery was required in order to compensate for the system losses such as power electronics. For the charging process less power on the battery was observed caused by the system losses.

The difference between ΔP at 0% SOC and 100% SOC was negligible. Although there is a known voltage dependency on SOC for battery systems, no significant effect was observed here. Even the higher currents at low SOC during constant power mode which could have affected the electronic parts on the DC side showed no influence. Also in this case, SOC-dependency at the same power level was insignificant.

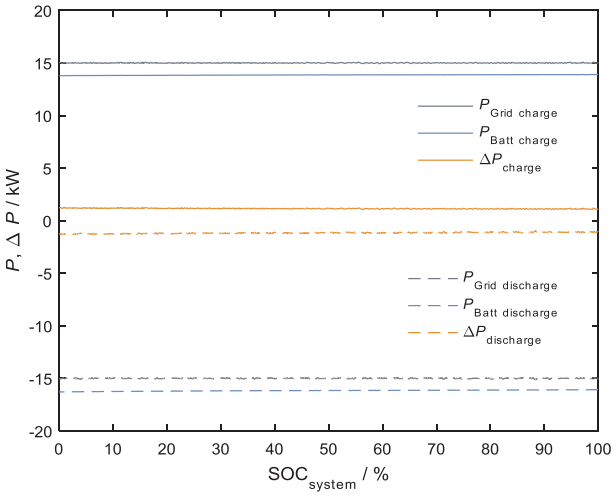

Fig. 5. Influence of SOC dependant efficiency difference obtained for system A. The blue lines are the constant power at the battery, whereby the dashed line is for discharge and the solid for charge. The grey lines are power demand (charging solid line) or delivery (discharging dashed line) on grid. The orange lines are the delta between power on grid and Li-ion battery storage, which describes the efficiency over the SOC-range. (For interpretation of the references to colour in this figure legend, the reader is referred to the web version of this article.)

The ΔP between charge and discharge was also rather independent from the state of charge. The battery part of overall efficiency illustrated in Fig. 4 did not have a high impact on overall efficiency. Only at higher power levels an increased influence could be seen and the impact on system losses increased. The influence of the state of charge difference on the complete battery energy storage system efficiency was negligible, although various effects influence the system. In addition the presented measurement procedure at one specific SOC in order to represent the complete system was quiet reasonable.

One additional system information for operating the battery energy storage systems are the standby losses. In Table 2 the losses from system A at different system states and supply source are shown. Table 2 includes the equivalent information for system B. System A had three different system operation states, in all of them standby losses occurred. The system state 'Off' during connection to the grid, resulted in an energy consumption of 22 W in order to support safety protection management systems such as the battery management system.

If the system is 'On', which meant the system could supply power to or from the grid, the energy consumption increased up to 115 W with an additional energy consumption of about 95 W from the battery system. In a special cooling mode (On, max. cooling) the system operated with high cooling rates for maximum power applications. Further system states such as Standby or Sleeping mode were not implemented for operation yet.

System B had three different system states in its original setup. Improvements after the detailed investigation lead to a significant increase in performance. The values for the energy losses during different operation modes are listed in Table 3. In the system state 'Off' no power was provided on the grid. In this case 80 W from the grid was needed to provide safety protection systems with energy. The second state was 'On', which meant ready for power supply. In this case still 80 W from the grid were needed plus 440 W from the battery system. The third mode is called 'On/standby' mode. In this case the inverter was in sleep mode, but the system was almost ready to deliver power instantaneously. In the system state 'On/standby' 12 W from the battery system were measured to supply BMS with energy and 100 W from grid were measured in order to support the control units. A further refinement of System B would decrease the energy consumption due to technical improvements (reduction of hardware components by means of enhanced control and energy management) by almost 50%. The values for the improved system were not validated in detail yet, but are shown for comparison in Table 3.

Table 2
The Standby and auxiliary losses of the system A on battery and at the grid in different system states.

System state	Grid supply/W	Battery supply/W
Off	22	0
On	115	95
On (max. cooling)	210	121

Table 3
The standby and auxiliary losses of the system B on the battery system and the grid at different system states.

System state	Grid supply/W	Battery supply/W
Off	80	0
On	80	440
On (improved system)	50	220
On/Standby	100	12
On/standby (improved system)	50	12

The standby losses were an important part of the energy efficiency analysis of the battery storage systems. In the case of just storing energy, the system was not operating the whole time. The higher the standby losses were the lower the storage efficiency of the system was.

The losses of the system would reduce the efficiency. If the battery storage systems are used for grid support such as primary control reserve the same information is important for feasibility studies, shown in the simulation part. The differentiation between the battery and the grid supply is also of importance. If the power was supplied from the battery system it reduced the usable capacity if no recharge was scheduled.

4. System simulation

There are a lot of different battery models existing in literature such as mathematical models[40], detailed physical modeling [41], equivalent electrical circuits models [42,43] or mixed models [44,45]. Based on the application it is necessary to choose the appropriate model approach to fulfill the simulation requirements. However, in order to describe an overall system behavior a common approach has to be applied. Battery cells are only a minor part of the battery system and an even smaller part of the overall storage system regarding energy losses. In this paper the efficiency of the overall system was separated into the battery system and the electric part for the system understanding. In the following section, the overall efficiency of the system was utilized for the simulation of decentralized battery storage systems for the application in the primary control reserve market. It offered the opportunity to optimize the virtual storage power based on the efficiency of the storage systems.

Based on this, only empirically derived mathematical models were used. For the model the root extraction of efficiency was used to distinguish between charge and discharge process. This model assumed a symmetric efficiency behavior of charging and discharging.

Two different functions were used to describe the overall efficiency of battery storage system A and B. The mathematically function were empirically derived. Both functions are valid for the range above 1 kW for charging and discharging, which is beyond the deadband for primary control reserve. For the system A the following mathematical function was used to describe the total efficiency of the battery storage system.

$$\eta_{\text{total}}(P) = \frac{\text{AB}}{(P - \text{AC})} - \text{D}\left(\frac{\text{A}}{P}\right)^2 \tag{8}$$

P is the power in kW and A, B, C and D are coefficients Table 4 in order

Table 4
Determined coefficients of the mathematical efficiency function from system A and system B.

Coefficient	System A	System B
A	139.59	110.15
B	198.76	1.5293
C	−2.3156	−0.98577
D	$4.5948 \cdot 10^{-4}$	

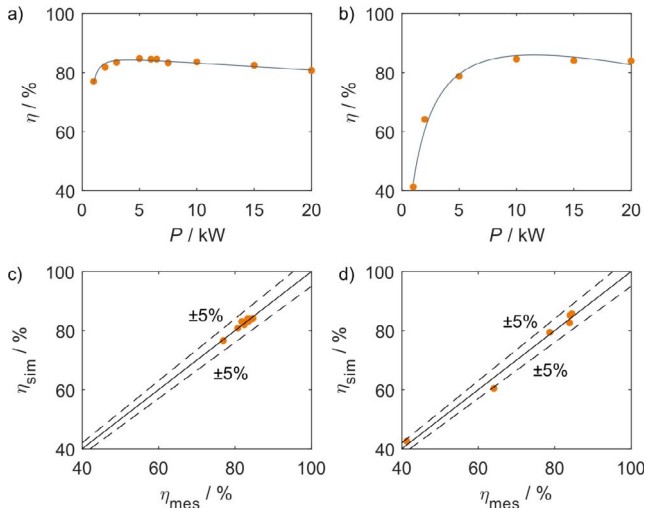

Fig. 6. The subplot (a) is the measured data and the efficiency fit considering equation of system A. The subplot (b) is the measured data and the efficiency fit considering the equation of system B. The subplot (c) is the parity plot of simulation data compared to measured data including 5% error range. The subplot (d) is the parity plot of simulation data compared to measured data including 5% error range.

to describe the function.

For system B the following equation was used to describe the overall efficiency.

$$\eta_{\text{total}}(P) = \frac{\text{A}P}{\text{B}+P} + \text{C}P \tag{9}$$

where P in kW is the active power and A, B and C are coefficients in order to describe the function shown in Table 4.

The used mathematical functions efficiently reflected the measurements with regard to the accuracy illustrated in Fig. 6 (c) and (d) in order to describe the total battery system efficiency of system A in subplot (a) and for system B in subplot (b). The parity plot describes the deviation of the simulated (η_{sim}) efficiency compared to the measured (η_{mes}) ones. Both functions were within the ± 5% error ranges. The measured values described the round trip efficiency.

For the simulation the measured frequency data of the synchronous grid of continental Europe [46] were used. These data were measured every 10 s. Based on the frequency data the needed active power supply to or from grid was determined. This was followed by the determination of the real power on battery for each system with respect to the power dependant total battery system efficiency. The difference was the loss while processing.

The simulation of the investigated battery systems A and B providing primary control reserve was carried out for two different months. The first month was February 2015 which represents the grid behavior during winter time and the second month was August 2015 which represents the grid behavior during summer time. Other than the power dependency of the battery storage system efficiency, also the grid conduct was considered to understand, predict and reduce system losses. During winter time the share of PV was less compared to the summer. The forecast accuracy was also lower compared to the summer

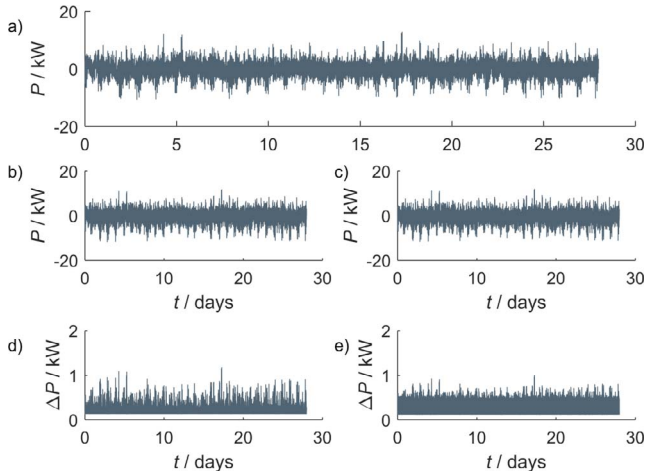

Fig. 7. Primary control reserve simulation results using real frequency data measured in February 2015. (a) Received power demand profile for primary reserve control. (b) Received power profile considering the efficiency of system A on the battery side. (c) Received power profile considering the efficiency of system B on the battery side. (d) Received additional power demand profile to compensate the efficiency losses for system A on the battery side. (e) Received additional power demand profile to compensate efficiency losses for system B on the battery side.

season caused by weather fluctuation, which had an impact on the frequency variation.

In Fig. 7 the results of the simulation with frequency data of February 2015 are shown. Subfigure (a) shows the active power on the grid side to fulfill the primary control reserve demand with respect to Fig. 3. The positive power in this graph describes the positive frequency deviation with a surplus of energy in the grid. It is called negative primary control reserve in order to balance the grid. The positive primary control reserve occurred during negative frequency deviation and resulted from an undersupply of energy in the grid. In this case during positive primary control reserve the system was discharged. The graphs (b) for system A and (c) for system B show the power on the battery side, whereby also positive power was a charge process and negative power was a discharge process. The subplots (d) for system A and (e) for system B show the overall losses, which occurred during operation. If the frequency was within the deadband, where no power from the system was required, the standby losses were used in the simulation.

System A and system B differed in the loss profiles. While system A showed higher losses at high power demand, system B showed a higher intermediate loss profile. The power profile furthermore shows that in many cases the power was below 10 kW, but with high fluctuations between 0 kW and 10 kW.

Table 5 is a summary of the simulation results and the results demonstrate that system A had lower losses compared to system B for the data of February 2015. The cumulated primary reserve total in kWh for February 2015 is the sum of negative primary reserve in kWh and the positive primary reserve in kWh. The primary reserve in kWh is derived by multiplying the primary reserve power with the timestep. The

Table 5
The simulation results with respect to frequency data of February 2015 including the total primary control reserve in sum, negative and positive. In addition the battery losses are shown.

	System A	System B
Primary reserve total/kWh	1026	
Primary reserve negative/kWh	516	
Primary reserve positive/kWh	510	
Energy loss total/kWh	142	214
Battery out/kWh	578	604
Battery in/kWh	470	422

battery power is mathematically connected to the primary reserve power via the power dependent efficiency η_{total} (P) at each individual time step. The efficiency η_{total} (P) is given in Eq. (8) for system A and in Eq. (9) for system B. Table 5 shows the calculated energies for the battery and the primary reserve for February 2015. For positive primary reserve one has to discharge the system, resulting in higher value of energy from the battery in order to compensate the losses of the storage system. For negative primary reserve one has to charge the system, resulting in lower value of the energy into the battery, because losses are also taken into account. The energy values of battery in and battery out are strictly dependent of the power profile resulting from frequency deviation due to power dependent efficiency. Energy loss total is the overall sum of the losses during operation and standby for both systems. Considering the energy in and out of the battery system, higher losses were detected for the system B. Calculating the efficiency based on energy in 470 kWh/422 kWh compared to energy out 578 kWh/604 kWh of the systems, system A had an overall efficiency of 81% and system B had an overall efficiency of 70%. It was also shown, that slightly more negative primary control reserve compared to the positive primary control reserve was needed in February 2015.

In Fig. 8 the simulation results of the theoretical primary control reserve considering the frequencies of August 2015 are shown. The subfigure (a) shows the required power on grid to fulfill the primary control reserve demands with respect to Fig. 3. The graphs (b) for system A and (c) for system B show the power on the battery side, where again the positive power was the charge process and negative power was the discharge process. The subplots (d) and (e) show the energy losses of system A and B. In contrast to the results based on the data of February 2015 the overall demand on primary control reserve was lower in August 2015. There were fewer peaks up to 10 kW with a less pronounced fluctuation in power demand.

In Table 6 the results were summarized. All values are derived as explained for Table 5. The total primary control reserve was 17% less compared to the February 2015 data. Also more positive primary control reserve was needed compared to more negative one in February 2015, probably due to the photovoltaic dominated summer season, but corresponding to the cloud-drift effect. System B had less energy losses compared to system A in August 2015. Considering the energy in and out of the battery systems higher losses were detected for system B again. Calculating the efficiency based on the energy in 371 kWh/327 kWh to the energy out 513 kWh/537 kWh of the systems, the system A had an efficiency of 72% compared to the efficiency of system B with a value of 61%.

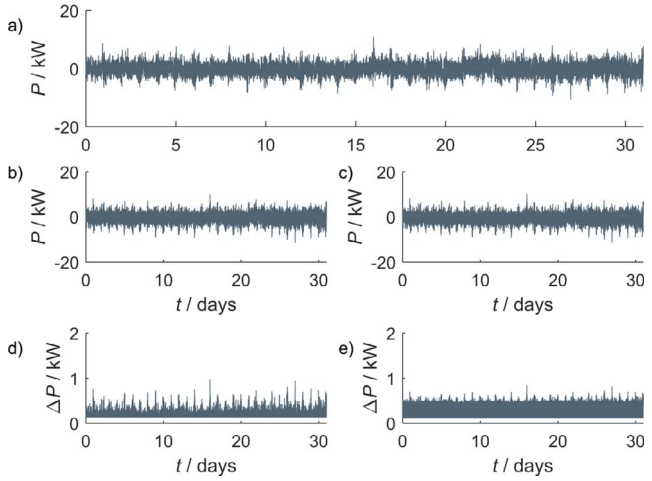

Fig. 8. Primary control reserve simulation results using real frequency data measured in August 2015. (a) Received power demand profile for primary reserve control. (b) Received power profile considering the efficiency of system A on the battery side. (c) Received power profile considering the efficiency of system B on the battery side. (d) Received additional power demand profile to compensate the efficiency losses at system A on the battery side. (e) Received additional power demand profile to compensate efficiency losses at system B on the battery side.

Table 6
The simulation results with respect to the frequency data of August 2015 including the total primary control reserve in sum, negative and positive. In addition, the battery losses are shown.

	System A	System B
Primary reserve total/kWh	850	
Primary reserve negative/kWh	409	
Primary reserve positive/kWh	441	
Energy loss total/kWh	148	210
Battery out/kWh	513	537
Battery in/kWh	371	327

Based on these results, system A had an improved performance, if frequency deviation was lower and the primary control reserve was at a lower average power level. System B showed an advantageous behavior at high frequency deviation and a higher average power level with respect to the primary control reserve. Referring to the results of Table 3 with the improved system B a recalculation could be done with the improved system behavior and the lower energy consumption. Due to the technical improvements the efficiency for February 2015 and August 2015 were 82% and 74% respectively. These results were higher compared to system A and the conventional system B. It is essential to investigate the system in the future, which was not done in detail yet.

In total system A showed an advantageous system behavior regarding primary control reserve, with regards to the frequency profiles in February and August 2015. If the frequency profile exhibited higher deviations from the standard frequency, system B was more efficient compared to system A, caused by higher efficiency in the higher power range. But even in February 2015 with higher demand on the primary control reserve compared to August 2015 system B had higher energy losses compared to system A. Both systems suffered from standby losses and low efficiency during periods with small demand of primary control reserve. A combination of various systems with optimized efficiency and enhanced standby modes would be beneficial to reduce these losses and enhance the operation behavior with respect to the primary control reserve for battery storage systems. Additionally, the technical improvements of system B lead to the assumption that the operation behavior of battery systems could be enhanced significantly.

5. Conclusion

The electrical and the energy efficiency behavior of two different battery storage systems were investigated. The standby and the auxiliary losses were determined. The efficiency measurement for the round-trip efficiency was shown at one specific state of charge point, which is representative for, the complete state of charge range. The overall battery storage system efficiency showed an insignificant dependency on the state of charge. Thus, the total battery system efficiency could be determined without carrying out full charge and discharge cycles. Furthermore the system efficiency, excluding the battery efficiency, was determined to be the predominant efficiency. This efficiency had a decisive influence on the overall efficiency of the battery storage systems and was responsible for the decrease of the latter. Due to the high power range between 0 and 20 kW the electronic devices could not perform over the complete range at the best operating point. At lower power level the auxiliary losses mainly influenced the energy efficiency, which was one key parameter to optimize the energy efficiency for operating at lower power level.

In addition simulations were carried out with respect to the primary control reserve. The total efficiency of a battery storage system specifically for grid support is a key parameter. Furthermore, the standby losses were taken into account and influence the overall efficiency of the system. The difference and the influence of the winter and the

summer season were described. The results also show the optimization potential for battery storage systems providing primary control reserve.

The next logical step would be to optimize the decentralized virtual storage plants based on these findings. Control systems for each single system, which support the grid by primary control reserve, to reduce the overall energy consumption would be a consequence. A combination of various systems with optimized efficiency and improved stand-by modes would be beneficial to reduce the losses and enhance the operation behavior with respect to primary control reserve application for battery storage systems.

Acknowledgment

The authors thank Dr. Jan-Jaap Rabbers for fruitful discussions. Also, the authors thank Caterva GmbH for helpful discussions regarding the operation of the virtual energy storage plant with decentralized battery storage systems. The work was partly financial supported by the public research program IET-1401-0004.

References

[1] International Energy Agency. World Energy Outlook 2014. London, 12. November 2014.
[2] McLellan B, Florin N, Giurco D, Kishita Y, Itaoka K, Tezuka T. Decentralised energy futures: the changing emissions reduction landscape. Proc CIRP 2015;29:138–43.
[3] Raghami A, Ameli MT, Hamzeh M. Primary and secondary frequency control in an autonomous microgrid supported by a load-shedding strategy. In: 4th Power electronics, drive systems and technologies conference (PEDSTC); 2013. p. 282–7.
[4] Amamra S-A, Francois B, Lugaro J. Day-ahead primary power reserve planning and day-D primary frequency control of a Li-ion battery. IEEE Eindhoven PowerTech 2015:1–5.
[5] Chen M, Rincón-Mora G. Accurate electrical battery model capable of predicting runtime and I-V performance, 2th. IEEE Trans Energy Convers 2006;21:504–11.
[6] Perez H, Siegel J, Lin X, Stefanopoulou A, Ding Y, Castanier M. Parameterization and validation of an integrated electro-thermal cylindrical LFP battery model. In: ASME 2012 5th annual dynamic systems and control conference joint with the JSME 2012 11th motion and vibration conference, Florida; 2012. p. 1–10.
[7] Vetter J, Novák P, Wagner MR, Veit C, Möller K-C, Besenhard JO, et al. Ageing mechanisms in lithium-ion batteries. J Power Sources 2005;14:269–81.
[8] Safari M, Morcrette M, Teyssot A, Delacourt C. Multimodal physics-based aging model for life prediction of Li-ion batteries. J Electrochem Soc 2009;156:A145–53.
[9] Buchberger I, Seidlmayer S, Pokharel A, Piana M, Hattendorf J, Kudejova P, et al. Aging analysis of graphite/$LiNi_{1/3}Mn_{1/3}$ $Co_{1/3}O_2$ cells sing SRD, PGAA, and AC impedance. J Electrochem Soc 2015;162(14):A2737–46.
[10] Barré, Deguilhem B, Grolleau S, Gßerard M, Suard F, Ríu D. A review on lithium-ion battery ageing mechanisms and estimations for automotive applications. J Power Sources 2013;241:680–9.
[11] Kassem M, Bernard J, Revel R, Pélissier S, Duclaud F, Delacourt C. Calendar aging of a graphite/$LiFePO_4$ cell. J Power Sources 2012;208:296–305.
[12] Käbitz S, Gerschler JB, Ecker M, Yurdagel Y, Emmermacher B, Andrße D, et al. Cycle and calendar life study of a graphite/$LiNi_{1/3}Mn_{1/3}Co_{1/3}O_2$ Li-ion high energy system. Part A: full cell characterization. J Power Sources 2013;239:572–83.
[13] Cho IH, Kim SS, Shin SC, Choi NS. Effect of SEI on capacity losses of spinel lithium manganese oxide/graphite batteries stored at 60 °C. Electrochem Solid-State Lett 2010;13:A168–72.
[14] Anseán D, Gonzaléz M, Viera JC, García VM, Blacno C, Valledor M. Fast charging technique for high power lithium iron phosphate batteries: a cycle life analysis. J Power Sources 2013;239:9–15.
[15] Bodenes L, Naturel R, Martinez H, Dedryvére R, Menetrier M, Croguennec L, et al. Lithium secondary batteries working at very high temperature: capacity fade and understanding of aging mechanisms. J Power Sources 2013;236:265–75.
[16] Joglekar MM, Ramakrishnan N. Cyclic capacity fade plots for aging studies of Li-ion cells. J Power Sources 2013;230:143–7.
[17] Liu P, Wang J, Hicks-Garner J, Sherman E, Soukiazian S, Verbrugge M, et al. Aging mechanisms of $LiFePO_4$ batteries deduced by electrochemical and structural analyses. J Electrochem Soc 2010;157:A499–507.
[18] Ramana CV, Mauger A, Gendron F, Julien CM, Zaghib K. Study of the Li-insertion/extraction process in $LiFePO_4/FePO_4$. J Power Sources 2009;187(2):555–64.
[19] Tarascon JM, Mckinnon WR, Coowar F, Bowmer TN, Amatucci G, Guyomard D. Synthesis conditions and oxygen stoichiometry effects on Li insertion into the spinel $LiMn_2O_4$. J Electrochem Soc 1994;141:1421–31.
[20] Gabrisch H, Tanghong Y, Yazami R. Transmission electron microscope studies of $LiNi_{1/3}Mn_{1/3}Co_{1/3}O_2$ before and after long-term aging at 70° C. Electrochem Solid-State Lett 2008;11:A119–24.
[21] Liu W, Delacourt C, Forgez C, Pelissier S. Study of graphite/NCA Li-ion cell degradation during accelerated aging tests – data analysis of the SimStock Project. IEEE VPPC 2011:1–6.
[22] Kubiak P, Wolfahrt-Mehrens M, Edstörm K, Morcrette M. Review on ageing mechanisms of different Li-ion batteries for automotive applications. Helios Project; 2012.
[23] Watanabe S, Kinoshita M, Hosokawa T, Morigaki K, Nakura K. Capacity fading of $LiAl_yNi_{1-x-y}Co_xO_2$ cathode for lithium-ion batteries during accelerated calendar and cycle life tests (effect of depth of discharge in charge discharge cycling on the suppression of the micro-crack generation of $LiAl_yNi_{1-x-y}Co_xO_2$ particle). J Power Sources 2014;260:50–6.
[24] Muto S, Sasano Y, Tatsumi K, Sasaki T, Horibuchi K, Takeuchi Y, et al. Capacity-fading mechanisms of $LiNiO_2$-based lithium-ion batteries II. Diagnostic analysis by electron microscopy and spectroscopy. J Electrochem Soc 2009;156:A371–7.
[25] Yang X, Sun X, McBreen J. New findings on the phase transitions in $Li_{1-x}NiO_2$: in situ synchrotron X-ray diffraction studies. Electrochem Commun 1999;1:227–32.
[26] Berndt H, Hermann M, Kreye HD, Reinisch R, Scherer U, Vanzetta J. Transmission code 2007. VDN: Netz- und Systemregeln der deutschen Übertragungsnetzbetreiber; 2007.
[27] Zhu G, Wen K, Lv W, Zhou X, Liang Y, Yang F, et al. Materials insights into low-temperature performances of lithium-ion batteries. J Power Sources 2015;300:29–40.
[28] Wong D, Shrestha B, Wetz DA, Heinzel JM. Impact of high rate discharge on the aging of lithium nickel cobalt aluminum oxide batteries. J Power Sources 2015;280:363–72.
[29] Sandrine B, Blanchard P, Robert S. Investigation of aging mechanisms of high power Li-ion cells used for hybrid electric vehicles. J Power Sources 2011;196:6841–6.
[30] Gomadam PM, Weidner JW, Dougal RA, White RE. Mathematical modeling of lithium-ion and nickel battery systems. J Power Sources 2002;110:267–84.
[31] Li Y, Zhang B, Chen M, Yang D, Liu J. Investigation of the internal resistance in $LiFePO_4$ cells for battery energy storage system. In: IEEE 9th conference on industrial electronics and applications (ICIEA); 2014. p. 1596–600.
[32] Sreeramulareddy N, Senthil Kumar N. Implementation of floating output interleaved input DC-DC boost converter. IJE Trans C: Aspects 2015;28(9):1–9.
[33] Gowri Sankar PA, Udhayakumar K. A novel carbon nanotube field effect transistors based low-voltage DC-DC buck converter for maximum efficiency. Asian J Chem 2013;25:290–2.
[34] Experimental validation of high-voltage-ratio low-input-current-ripple converters for hybrid fuel cell supercapacitor systems. In: 8th IEEE transaction on vehicular technology, vol. 61; 2013. p. 3430–40.
[35] Chang C-H, Cheng C-A, Chang E-C, Cheng H-L. Design and implementation of a two-switch buck-boost typed inverter with universal and high-efficiency features. In: 9th Int. conf. power electronics-ECCE Assia, vol. 63; 2015. p. 2737–43.
[36] Zhang Y, Zgang Z, Yang G. A novel control method for photovoltaic grid-connected micro-inverters to achieve high efficiency in light load. In: 9th Int. conf. power electronics-ECCE Assia, vol. 63; 2015. p. 2826–31.
[37] Cieslik S, Boniewicz P. The impact of initial phases of higher harmonics of the supply voltage of a single-phase transformer on the power losses in its core. In: 9th International conference on compatibility and power electronics (CPE); 2015. p. 144–50.
[38] Goh T, Kim D, Jeong JJ, Park M, Kim SW. Robust observer for state-of-charge estimation of Li-ion battery with uncertainties. In: 2015 10th Asian control conference (ASCC); 2015. p. 1–6.
[39] Kim DH, Koo K, Jeong JJ, Goh T, Kim SW. Second-order discrete-time sliding mode observer for state of charge determination based on a dynamic resistance Li-ion battery model. Energies 2013;6:5538–51.
[40] Ramadass P, Haran B, White R, Popov BN. Mathematical modeling of the capacity fade of Li-ion cells. J Power Sources 2003;123:230–40.
[41] Ning G, Popov BN. Cycle life modeling of lithium-ion batteries. J Electr Soc 2004;151:A1584–91.
[42] Rahmoun A, Biechl H. Modelling of Li-ion batteries using equivalent circuit diagrams. Electr Rev 2012;88:152–6.
[43] Yu Z-L, Guo Y-L, Wang H-Y. Research on state of charge estimation of Li-ion battery based on SCKF-STF. Dianji yu Kongzhi Xuebao/Electr Mach Control 2013;17:70–6.
[44] Illig J, Ender M, Weber A, Ivers-Tiffée E. Modelling graphite anodes with serial and transmission line models. J Power Sources 2015;282:335–47.
[45] Ramadesigan V, Northrop PWC, De S, Santhanagopalan S, Braatz RD, Subramanian VR. Modeling and simulation of lithium-ion batteries from a systems engineering perspective. J Electr Soc 2012;159:R31–45.
[46] Le réseau de l'intelligence électrique; 2015. < https://clients.rte-france.com/lang/an/visiteurs/vie/vie_frequence.jsp > .